

# Kinome rewiring reveals AURKA limits PI3K-pathway inhibitor efficacy in breast cancer

Hayley J. Donnell<sup>1</sup>, James T. Webber<sup>1</sup>, Rebecca S. Levin<sup>2</sup>, Roman Camarda<sup>3</sup>, Olga Momcilovic<sup>3</sup>, Nora Bayani<sup>4</sup>, Khyati N. Shah<sup>1</sup>, James E. Korkola<sup>4</sup>, Kevan M. Shokat<sup>2,5</sup>, Andrei Goga<sup>3</sup>, John D. Gordan<sup>3\*</sup> and Sourav Bandyopadhyay<sup>1\*</sup>

**Dysregulation of the PI3K-AKT-mTOR signaling network is a prominent feature of breast cancers. However, clinical responses to drugs targeting this pathway have been modest, possibly because of dynamic changes in cellular signaling that drive resistance and limit drug efficacy. Using a quantitative chemoproteomics approach, we mapped kinome dynamics in response to inhibitors of this pathway and identified signaling changes that correlate with drug sensitivity. Maintenance of AURKA after drug treatment was associated with resistance in breast cancer models. Incomplete inhibition of AURKA was a common source of therapy failure, and combinations of PI3K, AKT or mTOR inhibitors with the AURKA inhibitor MLN8237 were highly synergistic and durably suppressed mTOR signaling, resulting in apoptosis and tumor regression in vivo. This signaling map identifies survival factors whose presence limits the efficacy of targeted therapies and reveals new drug combinations that may unlock the full potential of PI3K-AKT-mTOR pathway inhibitors in breast cancer.**

Mutations and aberrant signaling of the PI3K-AKT-mTOR pathway (PI3K pathway) is a prominent feature of breast cancer and many other cancer types. Genomic alterations of PI3K-pathway components including *PTEN*, *PIK3CA* and *AKT1* occur in over 60% of breast malignancies<sup>1</sup>. Despite this high prevalence, drugs targeting this pathway have demonstrated only modest responses across numerous clinical trials<sup>2,3</sup>. The clinical observation that most breast cancers fail to respond suggests that additional factors modulate cellular response and drive resistance. A prominent feature of this pathway is drug-induced signaling adaptation and feedback mechanisms resulting in suboptimal drug responses<sup>4-6</sup>. Therefore, it is likely that understanding and targeting these dynamic changes in signaling will be important for optimizing this class of agents.

In principle, the measurement of dynamic changes elicited by therapy can be used to develop novel drug combinations. Though previous efforts have focused on acute signaling changes leading to pathway reactivation and drug resistance<sup>4,7</sup>, a systematic comparison of global signaling changes with drug efficacy has not been performed. Such an analysis may reveal survival factors whose suppression is required for drug efficacy, and hence could reveal new combinatorial strategies to enhance therapeutic responses. Previous identification of such factors has led to the understanding that drug-induced activation of apoptotic machinery<sup>8,9</sup> and impairment of protein synthesis<sup>10</sup> is required for sensitivity to a wide variety of drugs. In the context of breast cancer, multiple efforts in the field have identified mTORC1 as a survival factor whose suppression is necessary for PI3K-pathway inhibitor sensitivity<sup>11,12</sup>. This observation has led to clinical trials combining PI3K and mTOR inhibitors, yet reported clinical results have yielded suboptimal outcomes as a result of increased systemic toxicity and cytostatic tumor effects<sup>3</sup>. Hence, there remains a pressing need to uncover new combination

targets in order to improve therapeutic efficiency of PI3K-pathway inhibitors. Identifying additional survival factors will require a comprehensive understanding of signaling dynamics in response to treatment and insight as to how these dynamics contribute to drug resistance.

Little is known about global kinome rewiring in response to drug treatment, due in part to limitations in available technologies. Recently, a kinase-enrichment strategy has been developed using a chemoproteomics technique that combines kinase affinity capture with quantitative mass spectrometry (MS). This approach uses a multiplexed set of type I kinase inhibitors immobilized onto beads (multiplexed inhibitor beads, MIBs), which are used to affinity purify a diverse set of active kinases through their increased avidity for ATP compared to inactive kinases. Enriched kinases are then identified and quantified by LC-MS/MS (MIBs/MS), enabling simultaneous measurement of many endogenous kinases based on their activity state and abundance<sup>7</sup>. Because many drugs impinge on common pathways, and cell lines often display unique behaviors, it is possible that a quantitative map of kinase dynamics spanning multiple cell lines and drug treatments may be used to identify more general responses to drug treatment that are linked to drug sensitivity.

Here we applied the MIBs/MS approach to identify signaling changes associated with drug efficacy by mapping the kinome following exposure to targeted therapies across a panel of breast cancer cell lines of various subtypes and genotypes. Comparison of kinome activity profiles between drug-sensitive and resistant cells allowed us to generate a kinome-response signature associated with drug sensitivity. By performing a systematic analysis of signaling dynamics following drug treatment, we identified that failure to inhibit AURKA was associated with resistance to a diverse set of targeted therapies. Further analysis revealed that inhibition of AURKA was

<sup>1</sup>Department of Bioengineering and Therapeutic Sciences, University of California San Francisco, San Francisco, CA, USA. <sup>2</sup>Department of Cellular and Molecular Pharmacology, University of California San Francisco, San Francisco, CA, USA. <sup>3</sup>Department of Medicine, University of California San Francisco, San Francisco, CA, USA. <sup>4</sup>Center for Spatial Systems Biology, Oregon Health and Sciences University, Portland, OR, USA. <sup>5</sup>Howard Hughes Medical Institute, University of California San Francisco, San Francisco, CA, USA. \*e-mail: [john.gordan@ucsf.edu](mailto:john.gordan@ucsf.edu); [sourav.bandyopadhyay@ucsf.edu](mailto:sourav.bandyopadhyay@ucsf.edu)

sufficient to engender strong synergistic responses when combined with inhibitors of PI3K, AKT or mTOR. This provides an effective new framework for the unbiased identification of survival factors acting as molecular barriers to the efficacy of drugs, and we demonstrate the utility of this approach by developing rational combination strategies to enhance responses to PI3K-pathway inhibitors in breast cancer.

## Results

**Generation and analysis of a dynamic kinome signaling map.** We applied an unbiased proteomic strategy to measure kinome rewiring in response to drug treatment. Kinome profiling was performed via a chemoproteomics approach using MIBs coupled with mass spectrometry (MIBs/MS). Our library of MIBs consists of a mixture of sepharose beads covalently linked to 12 kinase inhibitors ranging from moderately selective (for example, lapatinib or sorafenib) to pan-kinase inhibitors (for example, purvalanol B or staurosporine) for broad kinome coverage (Fig. 1a; Supplementary Fig. 1). Because type I kinase inhibitors preferentially bind kinases in their active conformation, kinase capture by MIBs under the stringent binding conditions used here is a function of kinase expression, the affinity of kinases for the immobilized inhibitors, and the activation state of the kinase<sup>13</sup>. DMSO or drug-treated cell lysates were incubated with MIBs, and enriched kinases were eluted and quantified by LC-MS/MS using label-free quantitation (see Methods)<sup>14</sup>. We estimate that our current approach is able to capture roughly 35% of highly expressed kinases in a given sample (Supplementary Fig. 2).

We applied this strategy to a panel of breast cancer cell lines of various subtype and genotype classifications and measured kinome dynamics following treatment with a panel of targeted therapies. Cell lines were chosen to maximize transcriptional diversity and span the major subtypes of breast cancer (Supplementary Fig. 3). All lines harbored mutations in PI3K-pathway genes including *PIK3CA* mutant MCF7 (ER<sup>+</sup>/PR<sup>+</sup>), BT20 (receptor negative) and T47D (ER<sup>+</sup>/PR<sup>+</sup>); *PTEN*-null BT549 (receptor negative); and *HER2*-amplified SKBR3 (HER2<sup>+</sup>) (Supplementary Fig. 4a). Cell lines were treated for 24 h with DMSO or kinase inhibitors relevant to breast cancer signaling, including the EGFR/HER2 inhibitor lapatinib (200 nM), the pan-class I PI3K inhibitor GDC-0941 (250 nM), the AKT inhibitor MK2206 (250 nM), and the MEK inhibitor PD0325901 (100 nM), and then profiled using MIBs/MS (Fig. 1a; Supplementary Fig. 4b). Together, we quantified changes across 151 kinases in total, with changes in 75 kinases present in over 75% (15/20) of the samples (Fig. 1b; Supplementary Dataset 1). Significant drug-induced changes (defined based on the log<sub>2</sub> fold change of drug versus DMSO treatment, logFC) were detected for 99 kinases at  $P < 0.001$ , corresponding to 66% of kinases measured, indicating that the drugs had widespread and significant impacts on global kinome dynamics.

To assess the quality and reproducibility of the MIBs/MS data, we initially compared biological replicates of SKBR3 (HER2<sup>+</sup>) cells treated with the dual EGFR/HER2 small-molecule inhibitor lapatinib. We observed a high correlation of 0.78 between replicates for identified kinases ( $P = 5 \times 10^{-26}$ ) (Fig. 1c). The MIBs/MS screening strategy also accurately captured activity inhibition of direct drug targets by lapatinib, indicated by the significant decrease in levels for EGFR (logFC = -5.8,  $P = 6 \times 10^{-5}$ ) and HER2 (-0.7,  $P = 1 \times 10^{-4}$ ) (Fig. 1c). We observed a decrease in MEK1 activity upon treatment with the MEK inhibitor PD0325901 in BT549 and MCF7 cells (logFC = -1.8 and -1.2, respectively; Fig. 1d). We also observed indirect pathway-specific events, such as a decrease in the activity of the mTOR effector kinase RPS6KB1 when treated with either the PI3K inhibitor GDC-0941 or the AKT inhibitor MK2206 in MCF7 cells (logFC = -3.5 and -2.3, respectively; Fig. 1e). Comparison of observed kinome changes to previous MIBs/MS data revealed a high degree of concordance (Supplementary Fig. 5)<sup>15</sup>. These results

highlight the reproducibility of the MIBs/MS approach, as well as its ability to identify direct and indirect drug targets based on reductions in both activity and abundance.

We hypothesized that the identification of shared responses across lines and drugs may lead to a more robust understanding of signaling dynamics, as opposed to changes specific to a particular drug or cell type. We therefore sought to identify changes that were generally associated with sensitivity or resistance to treatment in a drug-agnostic fashion. First, cell lines were classified as sensitive or resistant to each of the drugs in our panel on the basis of dose-response analysis (Supplementary Fig. 4b; Supplementary Fig. 6a-d). Next, fold changes for each kinase were compared between these sensitive and resistant classifications for all drugs pooled together to identify candidate kinases whose inhibition was associated with drug sensitivity (Fig. 1f). This analysis revealed that suppression of 12 kinases was significantly associated with drug sensitivity ( $P < 0.05$ ). Among the identified candidates were kinases involved in cell-cycle processes, including mitotic kinases AURKA ( $P = 0.0001$ ) and CDK1 ( $P = 0.04$ ), and kinases involved in interphase, including CDK4 ( $P = 0.02$ ) and CDK2 ( $P = 0.05$ ). Other kinases identified were involved in YAP signaling (STK4,  $P = 0.01$ ) and WNT signaling (GSK3B,  $P = 0.005$  and CSNK1E,  $P = 0.02$ ). These results were not linked to general impairment of the cell cycle *per se*. We observed no correlation with sensitivity for other cyclin-dependent kinases (CDKs) measured in our screen such as CDK6, which is closely related to CDK4. In addition, the AURKA paralog AURKB was not significantly associated with sensitivity even though it is regulated during mitosis in a similar manner (Fig. 1f)<sup>16</sup>. We performed a similar analysis using a three-response categorization (i.e., sensitive, moderately sensitive and resistant) and found that these results were largely independent of the way sensitivity was classified (Supplementary Fig. 6e-g). We postulate that this drug-agnostic approach identifies changes that are general to drug sensitivity and reveals factors that may be missed by studies limited to a single-drug analyses. For example, the top candidate from our analysis, AURKA, was implicated but not found to be significantly associated with resistance or even among the top several candidates with any single drug. However, by pooling responses across all drugs it emerged as the one most associated with resistance in terms of both magnitude and significance (Supplementary Fig. 7). Therefore, by performing a systematic screen of signaling dynamics following drug exposure, we identified a set of specific kinases whose maintenance was associated with resistance to targeted therapies in breast cancer.

**AURKA associates with PI3K and AKT inhibitor resistance.** We focused our validation of molecular correlates of drug sensitivity on the PI3K pathway because of its central importance to breast cancer. We observed a significant association between maintenance of AURKA after treatment and drug resistance (Fig. 2a). To confirm this result, we measured molecular responses to treatment with the pan-PI3K inhibitor GDC-0941 in two sensitive (T47D and MCF7,  $IC_{50} < 200$  nM) and two new cell lines that were robustly resistant (HCC38 and MDAMB453,  $IC_{50} > 40$   $\mu$ M). A critical output of the PI3K pathway is the activation of the mTORC1 complex, whose inhibition is necessary for sensitivity to PI3K inhibitors<sup>11</sup>. After treatment we observed suppression of mTORC1 activity only in sensitive cells, as evidenced by decreased phosphorylation of its effector protein S6 (Fig. 2b). Confirming our MIBs/MS data, in response to treatment we observed decreases in the abundance and autophosphorylation of AURKA in sensitive cells, whereas resistant cells maintained these levels throughout (Fig. 2b; Supplementary Fig. 9a,b). Similar results were observed using the AKT inhibitor MK2206, representing the next step in the PI3K pathway (Supplementary Fig. 9c-e). These results confirm that failure to suppress AURKA activity is associated with resistance to PI3K and AKT inhibition in breast cancer cells.

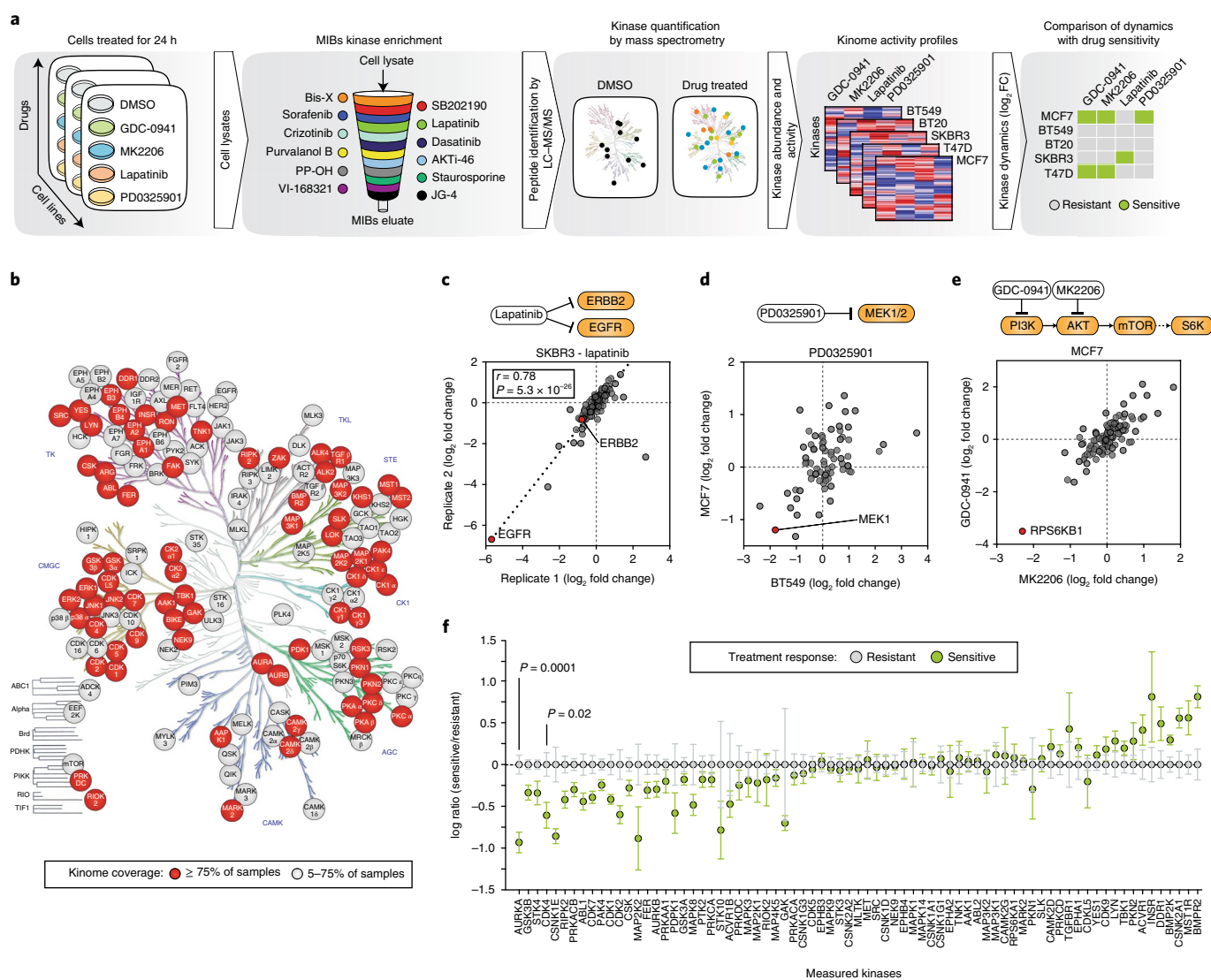


**Fig. 1 | Measurement of kinome dynamics to identify correlates of drug sensitivity.** **a**, Schematic of the approach using multiplexed inhibitor beads followed by MS (MIBs/MS). Sample lysates are passed through a column containing the indicated kinase inhibitors covalently linked to beads. After washing, bound proteins are eluted, trypsin digested and quantified through label-free MS. **b**, Human kinome tree annotated with kinases identified in this study, colored based on the percentage of total samples, whereby each particular kinase could be quantified. **c**, Comparison of activity ratios between biological replicates for 122 kinases, expressed as a log ratio of measurements from SKBR3 cells treated with 200 nM lapatinib for 24 h versus DMSO. Pearson correlation and  $P$  value are shown. **d**, Comparison of kinase activity ratios in BT549 and MCF7 cells treated with 100 nM PD0325901 versus DMSO. Data represent 75 kinases with one outlier kinase (GAK, BT549  $\log_2$  fold change 8.3) removed. **e**, Comparison of activity ratios for 70 kinases measured from MCF7 cells treated with either 250 nM MK2206 or GDC-0941 compared to DMSO. **f**, Categorical analysis of kinome dynamics occurring in drug-sensitive treatment responses ( $n = 6$ ) versus resistant treatment responses ( $n = 14$ ) for all drugs pooled together. For visualization purposes, each kinase was centered on the mean of resistant samples. Data are shown for 75 kinases, which could be measured in > 75% of samples. All drug treatments are 24 h. Error bars are mean  $\pm$  s.e.m., and  $P$  values were calculated using a two-sided  $t$ -test.

We next asked how AURKA is regulated in response to PI3K-pathway inhibition in drug-sensitive cells. AURKA regulates centrosome alignment, mitotic-spindle formation and chromosome segregation during mitosis, and its activity and abundance is tightly regulated<sup>16</sup>. We observed a robust and significant change in AURKA protein levels after 24 h in drug-sensitive cells, leading us to hypothesize that changes in transcription of AURKA might account for its loss after treatment. AURKA mRNA levels were decreased in response to GDC-0941 and MK2206 when comparing drug-sensitive and resistant cell lines ( $P = 2.8 \times 10^{-5}$  and  $P = 0.004$ , respectively; Fig. 2c,d). In addition, transcriptomes of MCF7 and T47D cells treated with the PI3K $\alpha$ -specific inhibitor BYL719 for 24 h<sup>17</sup> reflected a significant reduction of AURKA after drug

treatment in both of these BYL719-sensitive cell lines ( $IC_{50} \leq 250$  nM; Supplementary Fig. 10a)<sup>11,18</sup>. Interestingly, Gene Set Enrichment Analysis (GSEA)<sup>19</sup> of these transcriptomes revealed that a prominent component of the response to PI3K inhibition was the suppression of genes involved in the G2/M checkpoint, including AURKA, suggesting that transcriptional control of this aspect of the cell cycle is a major output of the PI3K pathway (Fig. 2e; Supplementary Fig. 10b; Supplementary Dataset 2).

**AURKA mediates survival during PI3K-pathway inhibition.** We next asked if the downregulation of AURKA was functionally relevant and whether the presence of AURKA limits efficacy of PI3K-pathway directed therapies. We tested whether AURKA inhibition

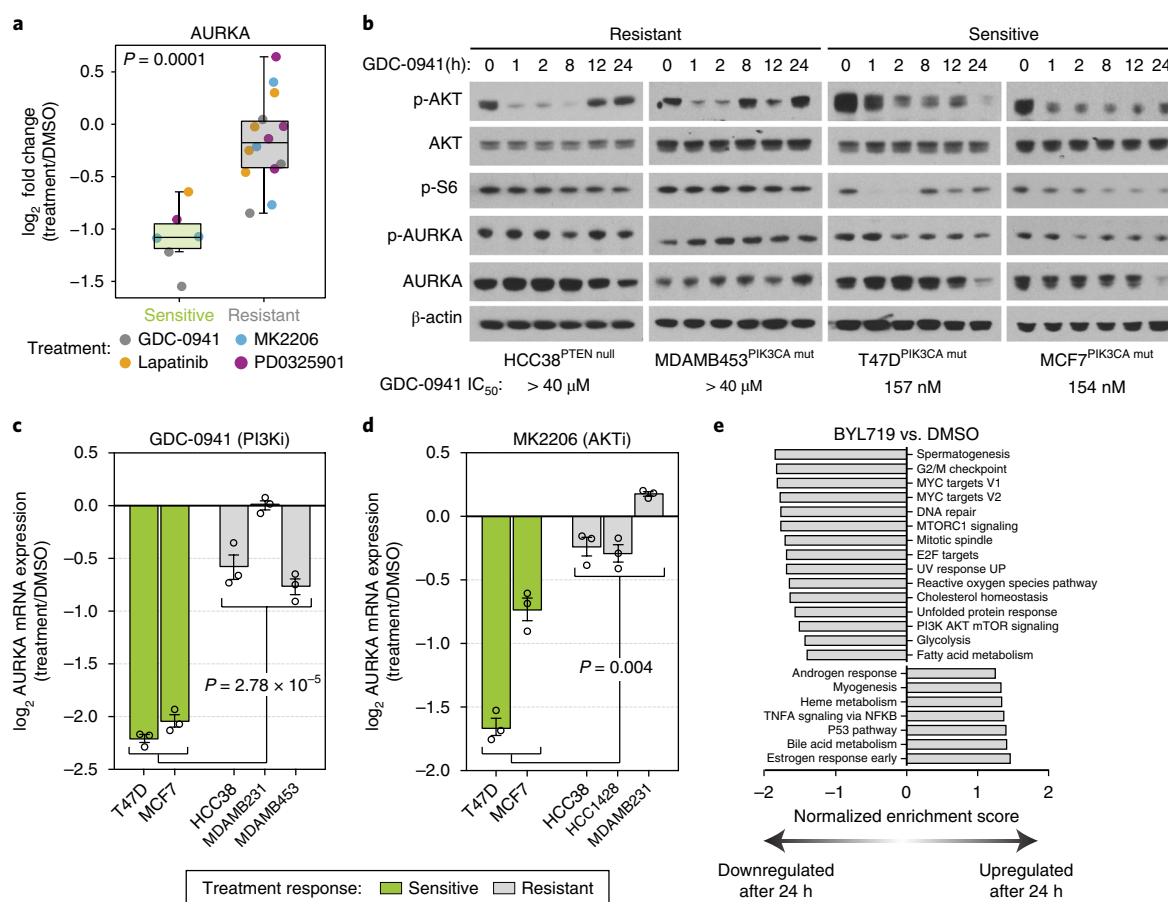


**Fig. 2 | Maintenance of AURKA is associated with resistance to PI3K inhibition.** **a**, Changes in activity of AURKA as measured by MIBs in drug-sensitive versus drug-resistant treatment responses after 24 h of exposure to the indicated compounds. Each point reflects a single cell line and drug treatment ( $n=20$  biologically independent samples). Box-and-whisker plots show median (centerline), upper/lower quartiles (box limits), and whiskers spanning the interquartile range from 25–75 percentiles.  $P$  value was calculated using a two-sided  $t$ -test. **b**, Western blot showing PI3K and AURKA signaling in GDC-0941-resistant and GDC-0941-sensitive cell lines. Protein lysates from cells treated with  $1\ \mu\text{M}$  GDC-0941 were extracted at different time points, separated by SDS-PAGE, and analyzed by immunoblot with the indicated antibodies. Image represents  $n=3$  independent experiments (full blots shown in Supplementary Fig. 8). **c,d**, Log ratio expression values of AURKA mRNA measured by RT-PCR from the indicated cell lines treated with  $1\ \mu\text{M}$  of GDC-0941 (**c**) or  $1\ \mu\text{M}$  MK2206 (**d**) for 24 h compared to DMSO treatment. Data represents  $n=3$  biological replicates. Error bars are mean  $\pm$  s.e.m., and  $P$  values were calculated using one-way ANOVA. **e**, Gene Set Enrichment Analysis (GSEA) of top gene sets significantly upregulated or downregulated after 24 h in response to  $1\ \mu\text{M}$  BYL719 treatment in MCF7 and T47D cells compared to DMSO. Data in **e** were based on transcriptomic data from Bosch et al.<sup>17</sup>. PI3Ki, PI3K inhibitor; AKTi, AKT inhibitor.

was sufficient to confer sensitivity to PI3K-pathway inhibitors using a combination-profiling approach to measure drug synergy across an extended panel of 13 breast cancer cell lines. We applied a dose matrix of increasing concentrations of the AURKA-specific inhibitor MLN8237 alone and in combination with a PI3K (GDC-0941), AKT (MK2206) or mTOR (RAD001) inhibitor and measured the effects on cell proliferation. To evaluate drug synergy, we (1) visualized Loewe excess values, (2) scored combination index values measuring shifts in drug potency, (3) calculated synergy scores based on Loewe excess values and (4) visualized and scored combinations using a Bliss independence model<sup>20</sup> (see Methods). Our results in MCF7 cells indicated that MLN8237 in combination with GDC-0941, MK2206 or RAD001 was synergistic using all four approaches (Fig. 3a; Supplementary Figs. 11–13; Supplementary Dataset 3). By testing the combination of MLN8237 with GDC-0941 across the extended panel of cell lines, we found significant synergy based on the Loewe excess model in 38% of models (5/13) on the basis of a synergy score  $> 1$ , which we determined through simulation to represent a less than 5% chance of nonsynergy (i.e., FDR  $< 5\%$ ; Fig. 3b; Supplementary Fig. 11). We extended this analysis to drug

combinations of MLN8237 with either MK2206 or RAD001 and found significant synergy in 54% and 85% of models, respectively (Fig. 3b; Supplementary Figs. 12 and 13). Overall, we found no significant trend toward synergy based on *PIK3CA* or *PTEN* mutational status, but did observe slightly increased synergy in receptor-positive cell lines (ER<sup>+</sup> or HER2<sup>+</sup>;  $P=0.04$  for GDC-0941 and  $P=0.035$  for MK2206, based on a two-tailed  $t$ -test; Supplementary Dataset 3).

Because PI3K-pathway inhibitors are primarily cytostatic<sup>5,21</sup> and AURKA is known to regulate apoptosis<sup>22</sup>, we next asked whether AURKA inhibition could enhance responses to PI3K-pathway inhibitors by inducing cytotoxic responses. Across 12 cell lines, we found that the addition of MLN8237 caused an increase in apoptotic cell death (Fig. 3c) that was independent of the particular dose used (Supplementary Fig. 14a,b). This enhancement in cell death generally occurred in conditions in which synergy was also observed (Supplementary Fig. 14b). We compared this response with the combination of CDK4/6 and PI3K inhibitors which are known to be synergistic<sup>12</sup>. Although we observed synergy between PI3K, AKT and mTOR inhibitors and the CDK4/6 inhibitor

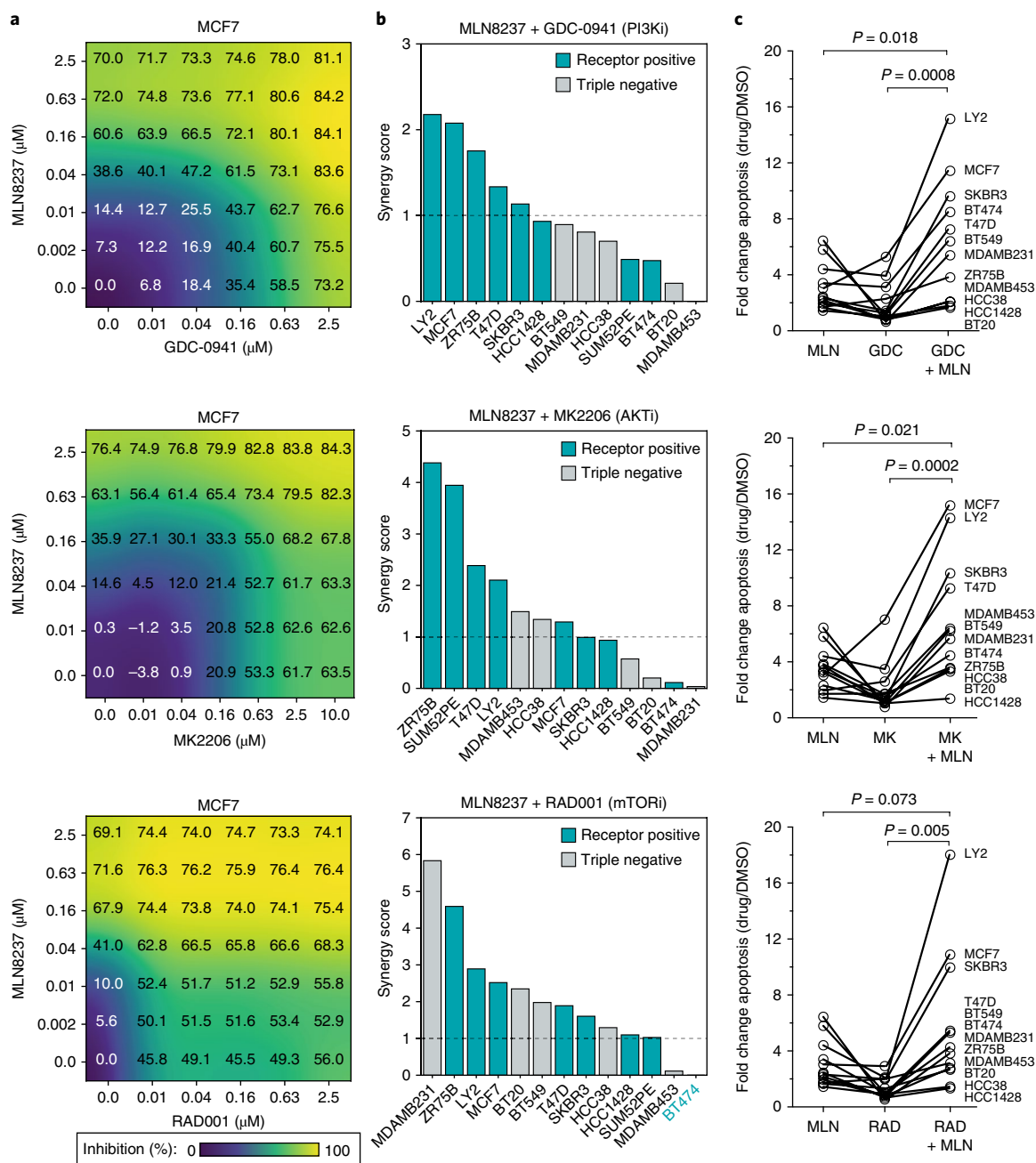


**Fig. 3 | AURKA suppression enhances sensitivity and drives cell death in response to PI3K-pathway inhibitors in breast cancer cell lines. a**, A dose matrix of GDC-0941 (PI3Ki), MK2206 (AKTi), or RAD001 (mTORi) in combination with the AURKA inhibitor MLN8237 in MCF7 cells. Cell proliferation was assessed after 72 h. Percent growth inhibition at each dose is shown. **b**, Synergy scores based on a Loewe excess inhibition model across 13 breast cancer cell lines that were treated with the indicated combinations using an escalating dose matrix for 72 h. Dashed line indicates a 5% FDR cutoff to define synergistic combinations (see Methods). **c**, Cell lines were treated with 625 nM of the indicated single agents or those combined together for 72 h, and apoptosis was measured by YO-PRO1 positivity. Data represents  $n = 4$  biologically independent samples. Error bars are mean  $\pm$  s.d., and  $P$  values were calculated using a two-sided  $t$ -test. PI3Ki, PI3K inhibitor; AKTi, AKT inhibitor; mTORi, mTOR inhibitor.

LEE011, the response was primarily cytostatic, indicating that CDK4 and CDK6 are only necessary for proliferation rather than for tumor cell survival in the presence of PI3K-pathway inhibitors (Supplementary Fig. 14c–e; Supplementary Dataset 3). Therefore, AURKA mediates cellular survival in the context of PI3K-pathway inhibition, and because the drug combinations are synergistic in inducing apoptosis in breast cancer cells, we propose that it may be a promising companion target to enhance the efficacy of PI3K-pathway inhibitors.

**MLN8237 and everolimus (RAD001) induce cell death in vivo.** We next evaluated the efficacy of this combination in vivo and focused on the combination of MLN8237 with the only FDA-approved inhibitor targeting this pathway in breast cancer, the mTOR inhibitor RAD001 (everolimus). Clinically, RAD001 overwhelmingly results in disease stabilization rather than regression<sup>23</sup>. This is reflected in vitro, wherein all lines have a high RAD001  $E_{\text{max}}$ , indicating cytostatic effects. In particular, MCF7 cells have a high  $E_{\text{max}}$  of 0.54 and do not display evidence of poly(ADP-ribose)

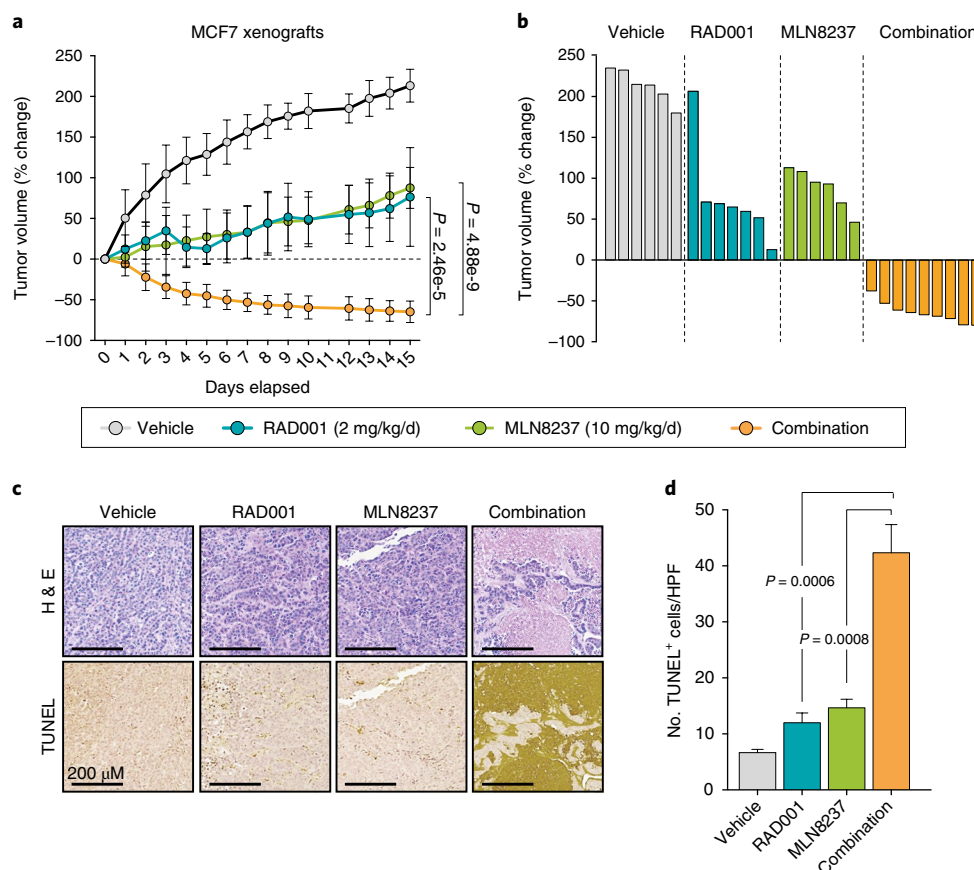


**Fig. 4 | The Aurora kinase inhibitor MLN8237 enhances sensitivity to everolimus (RAD001) and induces cell death in vivo.** **a**, MCF7 orthotopic xenograft tumors were treated with vehicle ( $n = 6$  biologically independent mice), RAD001 (2 mg/kg/day;  $n = 7$  biologically independent mice), MLN8237 (10 mg/kg/day,  $n = 6$  biologically independent mice) or with the combination of the two single agents ( $n = 9$  biologically independent mice) via oral gavage, daily, over 15 d. The percentage change in tumor volume was calculated for each animal from baseline. **b**, Individual tumor profiles compared to baseline for each tumor treated with vehicle ( $n = 6$  biologically independent mice), RAD001 ( $n = 7$  biologically independent mice), MLN8237 ( $n = 6$  biologically independent mice) or the combination ( $n = 9$  biologically independent mice) over a 15-d period. **c**, Representative images of tumor tissue extracted from mice after 15 d of treatment with the indicated agents and stained for H&E and TUNEL. Images are shown using a 10 $\times$  objective. Scale bars, 200  $\mu$ m. **d**, Quantification of the number of TUNEL<sup>+</sup> cells/field from TUNEL staining of MCF7 tumors following 15 d of treatment. Data is an average of five high-powered (20 $\times$ ) fields analyzed per tumor and are representative of  $n = 3$  biologically independent animals. In all graphs, error bars are mean  $\pm$  s.d., and  $P$  values were calculated using a two-sided  $t$ -test.

polymerase (PARP) cleavage at high doses (Supplementary Fig. 15). To investigate whether AURKA suppression enhances the response to RAD001 treatment, we tested the combination in MCF7 orthotopic transplants. Though RAD001 or MLN8237 monotherapy only partially impaired tumor growth, the combination showed significantly greater tumor growth inhibition than either single agent alone (Fig. 4a). Furthermore, all animals receiving the combination therapy (9/9) showed marked tumor regression, whereas no regressions were observed with monotherapy (0/13 in total;  $P = 2 \times 10^{-6}$  by Fisher's exact test; Fig. 4b). Post-treatment tumor specimens displayed an induction of apoptosis specific to the combination, as demonstrated by an increase in the number of TUNEL-positive cells (Fig. 4c,d). During the course of study, we did not observe any significant weight loss in animals receiving the combination as compared to the RAD001 single-agent group (Supplementary Fig. 16), suggesting tolerability and a lack of added toxicity from co-inhibiting Aurora kinase A. Therefore, addition of MLN8237 to RAD001 treatment results in tumor regression and a strong cytotoxic response in vivo.

**Co-inhibition durably suppresses mTORC1 signaling via AKT.** We next turned to identification of the mechanisms driving the

increased efficacy of the drug combination. Because most PI3K-pathway inhibitors (including rapamycin and RAD001) elicit feedback signals resulting in incomplete suppression of mTOR and drug resistance<sup>11,24</sup>, we first asked whether the combination of MLN8237 enhanced the activity of RAD001 on mTOR signaling to effectors RPS6 (S6) and 4E-BP1 in vivo. Though we observed an incomplete and partial suppression of S6 in RAD001-treated MCF7 xenografts, the addition of MLN8237 resulted in a durable and complete loss of S6 in all nine tumors (Fig. 5a). Though RAD001 is a relatively potent inhibitor of S6, it is a weak inhibitor of 4E-BP1, and therefore only partially impairs cap-dependent protein synthesis<sup>24</sup>. We thus investigated the activity of phospho-4E-BP1, which can be stimulated by rapamycin treatment<sup>24</sup>. Although phospho-4E-BP1 levels were enhanced with RAD001 single-agent treatment, co-treatment with MLN8237 suppressed these levels back to nearly baseline (Fig. 5a). This surprising finding led us to ask how Aurora kinase inhibition might alter this key signaling output of mTOR. We investigated AKT activity via phosphorylation of serine 473, which activates mTOR and is catalyzed by a variety of kinases<sup>25</sup>. Single-agent MLN8237 reduced phospho-AKT levels in both monotherapy and combination treatments, indicating that Aurora kinases sustain mTOR levels by promoting AKT activity (Fig. 5a). We next

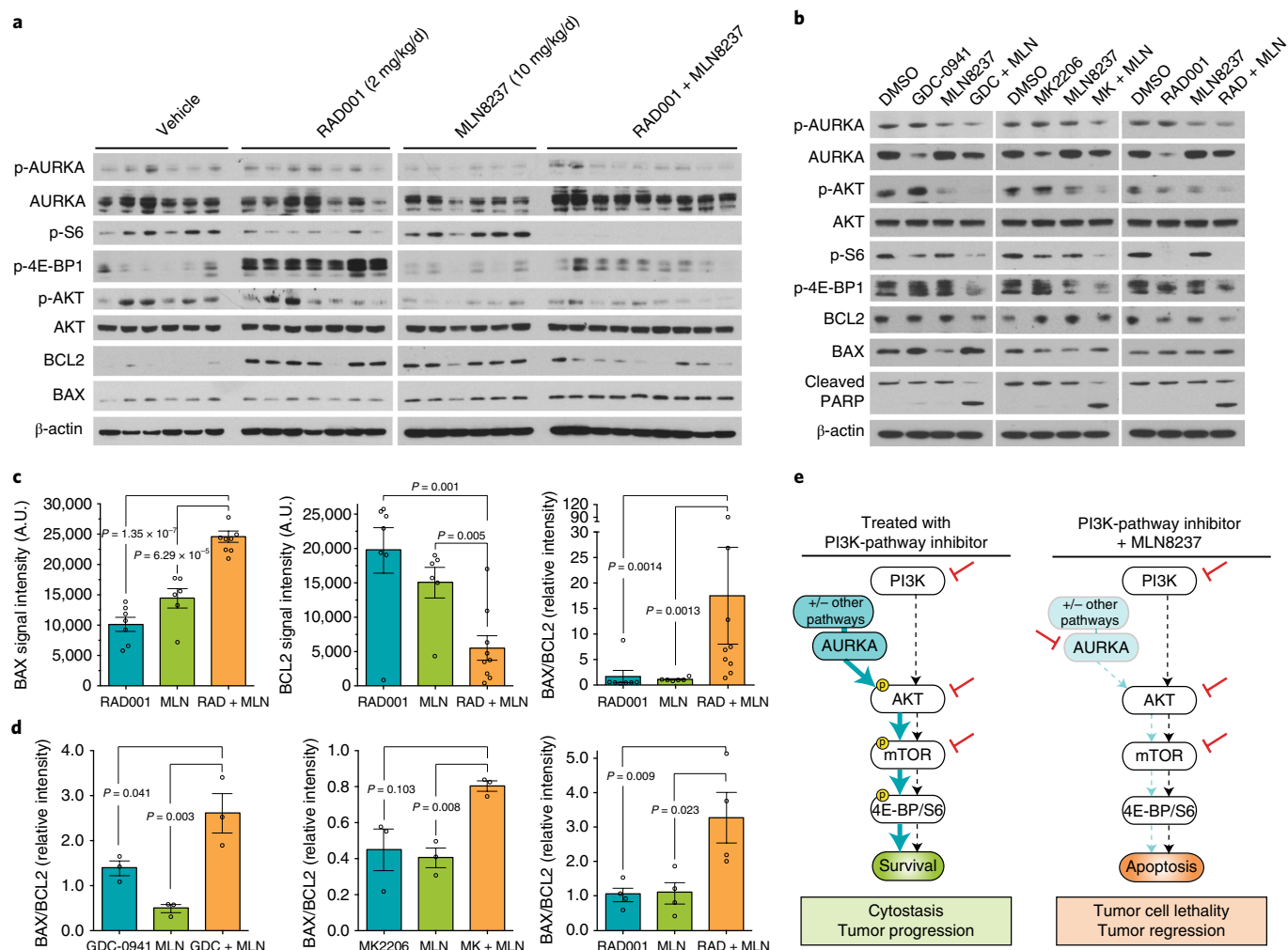


**Fig. 5 | Aurora kinase co-inhibition durably suppresses mTORC1 signaling and alters the BAX/BCL2 ratio.** **a**, MCF7 orthotopic xenografts were treated with vehicle ( $n=6$  biologically independent mice), RAD001 (2 mg/kg/day;  $n=7$  biologically independent mice), MLN8237 (10 mg/kg/day;  $n=6$  biologically independent mice) or the combination of the two single agents ( $n=9$  biologically independent mice) for 15 d, at which point tumors were harvested and snap frozen. Western blot of protein lysates from individual tumors were probed with the indicated antibodies (full blots shown in Supplementary Fig. 17a). **b**, MCF7 cells were treated with either 250 nM GDC-0941, 250 nM MK2206, 5 nM RAD001, 100 nM MLN8237 or the indicated combinations for 24 h, and protein lysates were subjected to immunoblot using the indicated antibodies. Representative image from  $n=3$  independent experiments (full blots shown in Supplementary Fig. 17b). **c**, BAX, BCL2 and BAX/BCL2 ratio in MCF7 orthotopic xenografts treated for 15 d with the indicated drugs based on quantification of western blot images (RAD001,  $n=7$ ; MLN8237,  $n=6$ ; combination,  $n=9$  biologically independent mice analyzed). **d**, BAX/BCL2 ratio in MCF7 cells treated for 24 h with the indicated drugs based on quantification of western blot images from  $n=3$  independent experiments. **e**, Proposed model of the mechanism of Aurora kinase inhibitor synergy. De novo resistance to single-agent inhibition of PI3K, AKT or mTOR is due to incomplete suppression of the pathway because of Aurora kinase signaling, which activates AKT. Drug combinations that simultaneously inhibit the PI3K pathway and block Aurora kinase signaling completely suppress mTOR signaling to 4E-BP1 and S6, resulting in tumor cell death. In all graphs, error bars are mean  $\pm$  s.e.m., and  $P$  values were calculated using a two-sided  $t$ -test.

examined whether Aurora-kinase-driven maintenance of mTOR was a general feature of PI3K-pathway inhibitors. Using MCF7 cells in vitro, we observed that MLN8237 treatment impaired phospho-AKT and that the combination of MLN8237 with either GDC-0941 (targeting PI3K) or MK2206 (targeting AKT) led to robust ablation of phospho-S6 and phospho-4E-BP1 levels (Fig. 5b). Therefore, Aurora kinases contribute to resistance to PI3K-pathway inhibitors through the maintenance of AKT and residual mTORC1 activity. Hence, targeting this survival mechanism results in a more durable and complete repression of the PI3K pathway.

**Co-inhibition unbalances pro- and antiapoptotic factors.** As we observed cell death in response to these drug combinations (Figs. 4d and 5b), we next sought to elucidate how Aurora kinase mediates

cell survival in response to PI3K-pathway suppression. Aurora kinases and mTOR both regulate a number of components of the intrinsic apoptosis pathway<sup>22,26</sup>, and we hypothesized that deregulation of the balance of pro- and antiapoptotic factors may cause cell death in response to drug combinations containing MLN8237. BAX promotes apoptosis, whereas BCL2 prevents apoptosis by inhibiting the activity of BAX, and together the balance of these two proteins forms a molecular rheostat for apoptosis<sup>27</sup>. In MCF7 xenografts, combination treatment resulted in an increase in BAX levels and a reduction in BCL2 levels, leading to an increase in the ratio of BAX/BCL2 compared to either MLN8237 or RAD001 treatment alone (Fig. 5c). Furthermore, the BAX/BCL2 ratio was also increased by the addition of MLN8237 to GDC-0941, MK2206 or RAD001 in MCF7 cells in vitro, in which it was associated with the presence

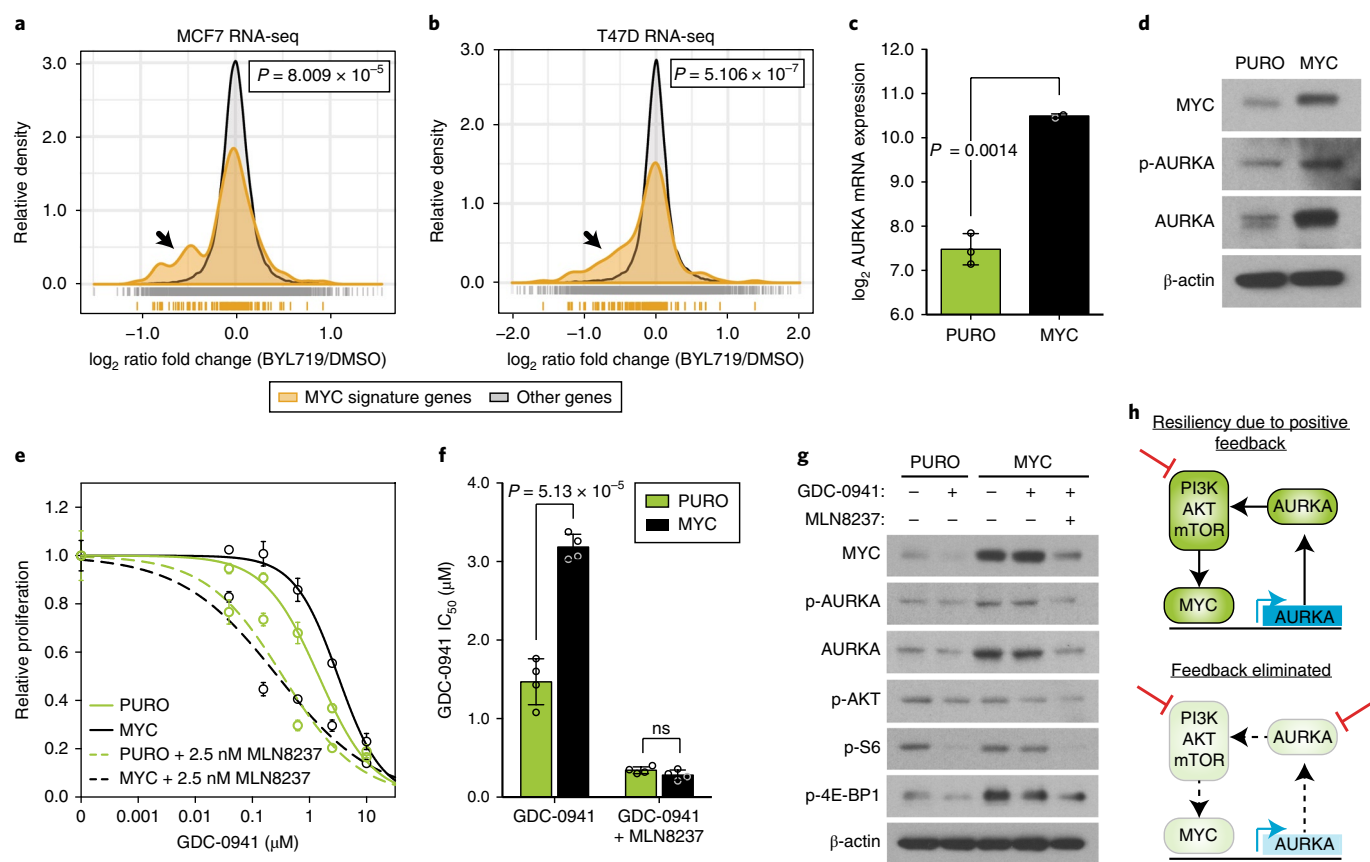


**Fig. 6 | AURKA transcription is regulated by MYC downstream of the PI3K pathway.** **a,b**, Histogram of normalized gene expression of all 150 genes in the MYC gene signature compared to genes not in this signature for MCF7 (**a**) or T47D (**b**) cells treated with  $1\mu\text{M}$  BYL719 or DMSO for 24 h. BYL719 treatment data were obtained from Bosch, et al.<sup>17</sup> and  $P$  values determined by Kolmogorov–Smirnov test. Black arrows highlight differences in distribution of MYC signature genes. **c**, Relative levels of AURKA mRNA in an isogenic pair of control (PURO,  $n=3$  independent samples) or MYC-expressing MCF10A cells ( $n=2$  independent samples) measured by RT-PCR. **d**, Immunoblot of protein lysates from PURO or MYC cells representative of  $n=3$  independent experiments with similar results (full blots shown in Supplementary Fig. 18a). **e**, Proliferation of control or MYC cells in response to GDC-0941 alone or in combination with 2.5 nM MLN8237. Combinations were normalized to MLN8237 alone. Data represent  $n=4$  biologically independent samples. **f**,  $\text{IC}_{50}$  analysis of dose-response curves shown in **e** from  $n=4$  independent samples. **g**, Immunoblot of lysates from control and MYC MCF10A cells treated with  $1\mu\text{M}$  GDC-0941 or 100 nM MLN8237 for 24 h. Representative image of  $n=3$  independent experiments with similar results (full blots shown in Supplementary Fig. 18b). **h**, Proposed model of positive feedback loop between the PI3K pathway, MYC and AURKA. In all graphs, error bars are mean  $\pm$  s.d., and  $P$  values were calculated using a two-sided  $t$ -test, unless otherwise indicated.

of cleaved PARP (Fig. 5b,d). Taken together, we propose a model whereby Aurora kinase inhibitors potentiate the activity of PI3K-pathway inhibitors by enabling a durable and complete suppression of AKT/mTOR signaling and drive cell death by altering the balance of pro- and antiapoptotic factors (Fig. 5e).

**MYC regulates AURKA downstream of the PI3K pathway.** We next sought to identify factors that regulate AURKA in response to PI3K-pathway inhibition. We noted that a MYC target gene signature was among the most suppressed gene sets after treatment with BYL719, suggesting that MYC may play a significant role in regulating the transcriptional response to PI3K inhibition and therefore potentially AURKA (Fig. 2e). To directly define whether MYC activity is suppressed by PI3K-pathway inhibition, we transcriptionally profiled an isogenic pair of MCF10A breast epithelial cells overexpressing MYC to derive a gene signature of the top 150 most upregulated genes by MYC (Supplementary Dataset 4). Comparison of this signature to transcriptional changes induced by BYL719 treatment in MCF7 and T47D cells revealed that most MYC signature genes were strongly repressed during PI3K inhibition (Fig. 6a,b). Therefore, MYC is regulated by the PI3K pathway in these cells, likely via mTORC1-mediated

translation and AKT-mediated stabilization of MYC<sup>28–30</sup>. AURKA was among the signature genes, and we found that MYC-overexpressing cells had an eight-fold increase in AURKA transcript levels as well as higher levels of total and phosphorylated AURKA protein (Fig. 6c,d). These data provide direct evidence that MYC regulates AURKA abundance and activity and suggest that both are controlled by the PI3K pathway in breast cancer.

Considering that AURKA activates AKT (Fig. 5b)<sup>31,32</sup>, our results suggest a model whereby the PI3K pathway regulates the abundance of its upstream activator AURKA through the control of MYC. Hence, MYC-driven AURKA signaling may constitute a positive feedback loop that helps to continuously activate the PI3K pathway, even in the context of single-agent drug treatment. In support of this theory, we observed that MCF10A-MYC cells were more resistant to GDC-0941 and MK2206 compared to parental cells, consistent with previous reports of MYC driving resistance to inhibitors of this pathway (Fig. 6e,f; Supplementary Fig. 19a,b)<sup>33–36</sup>. Although MYC-expressing cells were drug resistant, they could be resensitized to GDC-0941 or MK2206 by the addition of MLN8237 until they were back to approximately the same relative  $\text{IC}_{50}$  as parental cells with this combination (Fig. 6e,f; Supplementary Fig. 19a,b), indicating

that AURKA is principally responsible for causing the resistance to PI3K inhibition seen as a result of MYC activation in this model.

To test this model, we asked whether MYC-driven resistance to PI3K inhibitors occurs through the maintenance of PI3K-pathway activity and if this is dependent on AURKA. GDC-0941 treatment in MCF10A cells led to a reduction in MYC and AURKA signaling, as well as phospho-S6 and phospho-4E-BP1, indicating that MYC and AURKA are regulated by the PI3K pathway (Fig. 6g). However, constitutive expression of MYC resulted in the maintenance of all of these factors after PI3K inhibition, suggesting that MYC also acts upstream of the PI3K pathway and can maintain its activity. Furthermore, maintenance of mTORC1 signaling by MYC overexpression was reversed by co-inhibition of AURKA, thus designating AURKA as the critical link between MYC and activation of the PI3K pathway in these cells (Fig. 6g). Similar results were observed using the AKT inhibitor MK2206 (Supplementary Fig. 19c). Taken together, our data define a novel circuit whereby the PI3K pathway regulates the abundance of its own activator through MYC-mediated transcription of AURKA (Fig. 6h).

## Discussion

Through an unbiased proteomics approach to assay kinase activity, we measured dynamic changes elicited by therapy as a means to develop novel drug combinations. The systematic measurement of kinome dynamics across a diverse set of cell lines allowed us to map molecular changes associated with resistance to a variety of inhibitors, which is unique from previous approaches limited to a single drug or cell line<sup>7,15,37</sup>. We found a number of cases in which failure to inhibit a particular kinase was associated with drug resistance. As our proteomic screen included multiple drugs that impinge on distinct oncogenic pathways, we found it surprising that a set of common survival factors were identified. This may be due to the convergence of both the PI3K and MAPK pathways on protein synthesis<sup>38,39</sup>. Beyond AURKA, we identified that CDK4 suppression was associated with drug sensitivity and that the combination of CDK4 and PI3K-pathway inhibitors was synergistic, consistent with previous work<sup>12</sup>. Future work may determine if other candidates we identified also act as survival factors and how they might do so.

We show that the expression of AURKA limits the efficacy of PI3K-pathway-targeted therapy and thus represents a new vulnerability that can be used to enhance therapeutic responses to this class of drugs. By investigating AURKA regulation, we found that the reduction in AURKA abundance in drug-sensitive cells appears to be the result of transcriptional control by MYC, which is in turn regulated by the PI3K pathway. MYC has been shown to regulate AURKA transcription in multiple tumor types<sup>40–42</sup> and has independently been associated with resistance to PI3K inhibitors, which may be clinically relevant but remains mechanistically ambiguous<sup>33–36</sup>. Here we show that MYC-driven AURKA activation results in maintenance of the PI3K pathway despite PI3K inhibitor treatment, resulting in drug resistance. Future work may gauge the relative importance of AURKA relative to other outputs of MYC in driving resistance to PI3K inhibitors.

Maintenance of AURKA was sufficient to confer drug resistance in a variety of cell lines, as evident by the widespread drug synergy observed. We show that in response to treatment with PI3K-pathway inhibitors, Aurora kinase maintains the activation of AKT and drives residual mTOR activity. Co-inhibition of the PI3K pathway and AURKA with MLN8237 fully blocks this residual mTOR activity, resulting in cell death. These findings also highlight the importance of AKT activation through serine 473 as a route of drug resistance. Because a number of kinases have been shown to operate at this site, including mTORC2 (ref. 25), it remains unclear whether Aurora kinases act on this site directly or indirectly. These studies elaborate a positive feedback loop whereby the PI3K pathway promotes the expression of AURKA, which in turn activates the pathway via AKT. One feature of such a positive-feedback loop is

the creation of switch-like outputs resulting in heightened stability and resistance to perturbation<sup>43</sup>. We postulate that such loops are common and may lead to the resiliency and adaptation that is a hallmark of the PI3K pathway and a major cause of the challenges in targeting it therapeutically. Delineating such loops may be an important strategy in identifying effective drug combinations. As a case in point, we show that eliminating this positive-feedback loop by blocking AURKA renders cells more sensitive to PI3K inhibitors.

Our findings reveal that the combination of Aurora kinase inhibitors and PI3K-pathway inhibitors is synergistic and could be a promising clinical strategy to enhance the treatment response in breast cancer. These data are consistent with observations made in other settings<sup>44–46</sup>. Clinical data of PI3K and mTOR inhibitors have shown only modest benefit in breast cancers, at best resulting in short-term disease stabilization in patients<sup>23,47</sup>. Consistent with these clinical observations, most inhibitors in this class cause only a proliferative arrest *in vitro*<sup>5,21</sup> and it has been proposed that combinations that induce apoptosis may be used to enhance responses<sup>48</sup>. In contrast to cytostatic combinations with the CDK4/6 inhibitor (i.e., synthetic sickness), we found that combinations with Aurora kinase inhibitors were synergistic and potently induced cell death. As clinical trials testing CDK4/6 inhibitor combinations are ongoing, it remains to be seen what impact this distinction will play on patient responses. These results warrant an expanded analysis of combinations with AURKA inhibitors in additional patient-derived models of breast cancer and other cancer types. Tested as monotherapy, Aurora kinase inhibitors have reached phase 3 clinical trials for lymphoma with manageable toxicities but limited efficacy<sup>49</sup>. Given that the most common adverse events of PI3K-pathway inhibition are hyperglycemia, rash and gastrointestinal toxicity, and that those of Aurora kinase inhibition are primarily neutropenia, we are encouraged that the nonoverlapping toxicity profile between the two agents may be tolerated in patients as they were in our *in vivo* studies. As single-agent responses to both PI3K-pathway and Aurora kinase inhibitors have been modest, these findings may unlock the full potential of these agents in realizing a clinical benefit.

## Methods

Methods, including statements of data availability and any associated accession codes and references, are available at <https://doi.org/10.1038/s41589-018-0081-9>.

Received: 19 January 2018; Accepted: 13 April 2018;  
Published online: 25 June 2018

## References

1. Cancer Genome Atlas Network. Comprehensive molecular portraits of human breast tumours. *Nature* **490**, 61–70 (2012).
2. Janku, F. et al. Assessing PIK3CA and PTEN in early-phase trials with PI3K/AKT/mTOR inhibitors. *Cell Rep* **6**, 377–387 (2014).
3. Dey, N., De, P. & Leyland-Jones, B. PI3K-AKT-mTOR inhibitors in breast cancers: from tumor cell signaling to clinical trials. *Pharmacol. Ther.* **175**, 91–106 (2017).
4. O'Reilly, K. E. et al. mTOR inhibition induces upstream receptor tyrosine kinase signaling and activates Akt. *Cancer Res.* **66**, 1500–1508 (2006).
5. Klemperer, S. J., Myers, A. P. & Cantley, L. C. What a tangled web we weave: emerging resistance mechanisms to inhibition of the phosphoinositide 3-kinase pathway. *Cancer Discov.* **3**, 1345–1354 (2013).
6. Shah, P.D. & Chandarlapaty, S. in *PI3K-mTOR in Cancer and Cancer Therapy* (eds. Dey, N., De, P. & Leyland-Jones, B.) 125–147 (Springer International Publishing, 2016).
7. Duncan, J. S. et al. Dynamic reprogramming of the kinome in response to targeted MEK inhibition in triple-negative breast cancer. *Cell* **149**, 307–321 (2012).
8. Corcoran, R. B. et al. TORC1 suppression predicts responsiveness to RAF and MEK inhibition in *BRAF*-mutant melanoma. *Sci. Transl. Med.* **5**, 196ra98 (2013).
9. Anderson, G. R. et al. PIK3CA mutations enable targeting of a breast tumor dependency through mTOR-mediated MCL-1 translation. *Sci. Transl. Med.* **8**, 369ra175 (2016).

10. Boussemaert, L. et al. eIF4F is a nexus of resistance to anti-BRAF and anti-MEK cancer therapies. *Nature* **513**, 105–109 (2014).
11. Elkabets, M. et al. mTORC1 inhibition is required for sensitivity to PI3K p110 $\alpha$  inhibitors in PIK3CA-mutant breast cancer. *Sci. Transl. Med.* **5**, 196ra99 (2013).
12. Vora, S. R. et al. CDK 4/6 inhibitors sensitize PIK3CA mutant breast cancer to PI3K inhibitors. *Cancer Cell* **26**, 136–149 (2014).
13. Bantscheff, M. et al. Quantitative chemical proteomics reveals mechanisms of action of clinical ABL kinase inhibitors. *Nat. Biotechnol.* **25**, 1035–1044 (2007).
14. Sos, M. L. et al. Oncogene mimicry as a mechanism of primary resistance to BRAF inhibitors. *Cell Rep.* **8**, 1037–1048 (2014).
15. Stuhlmiller, T. J. et al. Inhibition of lapatinib-induced kinome reprogramming in ERBB2-positive breast cancer by targeting BET family bromodomains. *Cell Rep* **11**, 390–404 (2015).
16. Lens, S. M. A., Voest, E. E. & Medema, R. H. Shared and separate functions of polo-like kinases and aurora kinases in cancer. *Nat. Rev. Cancer* **10**, 825–841 (2010).
17. Bosch, A. et al. PI3K inhibition results in enhanced estrogen receptor function and dependence in hormone receptor-positive breast cancer. *Sci. Transl. Med.* **7**, 283ra51 (2015).
18. Leroy, C. et al. Activation of IGF1R/p110 $\beta$ /AKT/mTOR confers resistance to  $\alpha$ -specific PI3K inhibition. *Breast Cancer Res.* **18**, 41 (2016).
19. Subramanian, A. et al. Gene set enrichment analysis: a knowledge-based approach for interpreting genome-wide expression profiles. *Proc. Natl. Acad. Sci. USA* **102**, 15545–15550 (2005).
20. Fouquier, J. & Guedj, M. Analysis of drug combinations: current methodological landscape. *Pharmacol. Res. Perspect.* **3**, e00149 (2015).
21. Fruman, D. A. & Rommel, C. PI3K and cancer: lessons, challenges and opportunities. *Nat. Rev. Drug Discov.* **13**, 140–156 (2014).
22. Nikonova, A. S., Astsaturov, I., Serebriiskii, I. G., Dunbrack, R. L. Jr. & Golemis, E. A. Aurora A kinase (AURKA) in normal and pathological cell division. *Cell. Mol. Life Sci.* **70**, 661–687 (2013).
23. Piccart, M. et al. Everolimus plus exemestane for hormone-receptor-positive, human epidermal growth factor receptor-2-negative advanced breast cancer: overall survival results from BOLERO-2. *Ann. Oncol.* **25**, 2357–2362 (2014).
24. Choo, A. Y., Yoon, S.-O., Kim, S. G., Roux, P. P. & Blenis, J. Rapamycin differentially inhibits S6Ks and 4E-BP1 to mediate cell-type-specific repression of mRNA translation. *Proc. Natl. Acad. Sci. USA* **105**, 17414–17419 (2008).
25. Vadlakonda, L., Dash, A., Pasupuleti, M., Anil Kumar, K. & Reddanna, P. The paradox of Akt-mTOR interactions. *Front. Oncol.* **3**, 165 (2013).
26. Laplante, M. & Sabatini, D. M. mTOR signaling in growth control and disease. *Cell* **149**, 274–293 (2012).
27. Volkmann, N., Marassi, F. M., Newmeyer, D. D. & Hanein, D. The rheostat in the membrane: BCL-2 family proteins and apoptosis. *Cell Death Differ.* **21**, 206–215 (2014).
28. West, M. J., Stoneley, M. & Willis, A. E. Translational induction of the *c-myc* oncogene via activation of the FRAP/TOR signalling pathway. *Oncogene* **17**, 769–780 (1998).
29. Sears, R. et al. Multiple Ras-dependent phosphorylation pathways regulate Myc protein stability. *Genes Dev* **14**, 2501–2514 (2000).
30. Diehl, J. A., Cheng, M., Roussel, M. F. & Sherr, C. J. Glycogen synthase kinase-3 $\beta$  regulates cyclin D1 proteolysis and subcellular localization. *Genes Dev.* **12**, 3499–3511 (1998).
31. Yang, H., He, L., Kruk, P., Nicosia, S. V. & Cheng, J. Q. Aurora-A induces cell survival and chemoresistance by activation of Akt through a p53-dependent manner in ovarian cancer cells. *Int. J. Cancer* **119**, 2304–2312 (2006).
32. Dar, A. A., Belkhir, A. & El-Rifai, W. The aurora kinase A regulates GSK-3 $\beta$  in gastric cancer cells. *Oncogene* **28**, 866–875 (2009).
33. Martins, M. M. et al. Linking tumor mutations to drug responses via a quantitative chemical-genetic interaction map. *Cancer Discov.* **5**, 154–167 (2015).
34. Muellner, M. K. et al. A chemical-genetic screen reveals a mechanism of resistance to PI3K inhibitors in cancer. *Nat. Chem. Biol.* **7**, 787–793 (2011).
35. Ilic, N., Utermark, T., Widlund, H. R. & Roberts, T. M. PI3K-targeted therapy can be evaded by gene amplification along the MYC-eukaryotic translation initiation factor 4E (eIF4E) axis. *Proc. Natl. Acad. Sci. USA* **108**, E699–E708 (2011).
36. Liu, P. et al. Oncogenic PIK3CA-driven mammary tumors frequently recur via PI3K pathway-dependent and PI3K pathway-independent mechanisms. *Nat. Med.* **17**, 1116–1120 (2011).
37. Nomanbhoy, T. K. et al. Chemoproteomic evaluation of target engagement by the cyclin-dependent kinase 4 and 6 inhibitor palbociclib correlates with cancer cell response. *Biochemistry* **55**, 5434–5441 (2016).
38. Roux, P. P. et al. RAS/ERK signaling promotes site-specific ribosomal protein S6 phosphorylation via RSK and stimulates cap-dependent translation. *J. Biol. Chem.* **282**, 14056–14064 (2007).
39. She, Q.-B. et al. 4E-BP1 is a key effector of the oncogenic activation of the AKT and ERK signaling pathways that integrates their function in tumors. *Cancer Cell* **18**, 39–51 (2010).
40. den Hollander, J. et al. Aurora kinases A and B are up-regulated by Myc and are essential for maintenance of the malignant state. *Blood* **116**, 1498–1505 (2010).
41. Lu, L. et al. Aurora kinase A mediates *c-Myc*'s oncogenic effects in hepatocellular carcinoma. *Mol. Carcinog.* **54**, 1467–1479 (2015).
42. Zheng, F. et al. Nuclear AURKA acquires kinase-independent transactivating function to enhance breast cancer stem cell phenotype. *Nat. Commun.* **7**, 10180 (2016).
43. Ferrell, J. E. Jr. Self-perpetuating states in signal transduction: positive feedback, double-negative feedback and bistability. *Curr. Opin. Cell Biol.* **14**, 140–148 (2002).
44. Katscha, A. et al. Activation of EIF4E by aurora kinase A depicts a novel druggable axis in everolimus-resistant cancer cells. *Clin. Cancer Res.* **23**, 3756–3768 (2017).
45. Brewer Savannah, K. J. et al. Dual targeting of mTOR and aurora-A kinase for the treatment of uterine Leiomyosarcoma. *Clin. Cancer Res.* **18**, 4633–4645 (2012).
46. Liu, L.-L. et al. Inhibition of mTOR pathway sensitizes acute myeloid leukemia cells to aurora inhibitors by suppression of glycolytic metabolism. *Mol. Cancer Res.* **11**, 1326–1336 (2013).
47. Baselga, J. et al. Buparlisib plus fulvestrant versus placebo plus fulvestrant in postmenopausal, hormone receptor-positive, HER2-negative, advanced breast cancer (BELLE-2): a randomised, double-blind, placebo-controlled, phase 3 trial. *Lancet Oncol.* **18**, 904–916 (2017).
48. Zwang, Y. et al. Synergistic interactions with PI3K inhibition that induce apoptosis. *eLife* **6**, e24523 (2017).
49. Barr, P. M. et al. Phase II intergroup trial of alisertib in relapsed and refractory peripheral T-cell lymphoma and transformed mycosis fungoides: SWOG 1108. *J. Clin. Oncol.* **33**, 2399–2404 (2015).

## Acknowledgements

The authors would like to thank members of the Bandyopadhyay laboratory for helpful discussions and technical assistance. We also thank A. Beardsley, E. Markegard, D. Ruggero and W. Weiss for helpful discussions and reagents. This work was supported in part by NCI U01CA168370 (S.B.), NIGMS R01GM107671 (S.B.), NCI R01CA170447 (A.G.), Prospect Creek Foundation (S.B., A.G.), OHSU Pilot Project Funding (S.B., J.K.), American Cancer Society Postdoctoral Fellowship (J.D.G.), the Gazarian Foundation (A.G.), DOD W81XWH-12-1-0272 and DOD W81XWH-16-1-0603 (A.G.).

## Author contributions

H.J.D., J.T.W., K.M.S., J.K., J.D.G., and S.B. contributed toward study conceptualization. H.J.D., J.T.W., and J.D.G. performed data analyses supporting the study. H.J.D. designed and performed the majority of experiments. N.B. assisted with samples for initial MIBs/MS profiling. R.S.L., J.T.W., and J.D.G. provided technical advice and guided the interpretation of mass spectrometry data from MIB/MS profiling. R.C. and O.M. assisted with animal studies, and K.N.S. helped with additional experiments. H.J.D. and S.B. composed the original draft, and all authors contributed to manuscript finalization. S.B. and A.G. supervised the study.

## Competing interests

The authors declare no competing interests.

## Additional information

**Supplementary information** is available for this paper at <https://doi.org/10.1038/s41589-018-0081-9>.

**Reprints and permissions information** is available at [www.nature.com/reprints](http://www.nature.com/reprints).

**Correspondence and requests for materials** should be addressed to J.D.G. or S.B.

**Publisher's note:** Springer Nature remains neutral with regard to jurisdictional claims in published maps and institutional affiliations.

## Methods

**Breast cancer cell lines and reagents.** BT549 and SKBR3 cells were obtained from the UCSF Cell Culture Facility. BT20, BT474, HCC1428, HCC38, LY2, MCF7, MDAMB231, MDAMB453, T47D, SUM52PE, and ZR75B cell lines were obtained from the American Type Culture Collection (ATCC). Cell lines used for proteomic profiling and molecular analyses were authenticated by STR analysis. Lines were grown according to published protocols<sup>50</sup> except for SKBR3, which was cultured using RPMI media supplemented with 10% FBS and 1% pen/strep. All cell lines tested negative for mycoplasma contamination. Drugs used for cell culture experiments in this study were purchased from Selleck Chemicals (GDC-0941, MK2206, PD0325901, lapatinib, MLN8237, and LEE011) and LC Laboratories (RAD001).

**Multiplex inhibitor bead (MIB) analysis.** Multiplexed inhibitor bead enrichment and MS analysis (MIBs/MS) were performed as described previously<sup>14</sup>. In summary, a selection of bait compounds were purchased or synthesized and immobilized on sepharose using standard peptide coupling chemistry. The following compounds were purchased commercially: bisindolylmaleimide X (Enzo Life Sciences); SB202190, staurosporine (LC Labs); purvalanol B (Tocris); lapatinib, crizotinib, dasatinib (Selleckchem). When not commercially available without modification, linkable versions of previously described compounds were synthesized based on prior methods: VI-16832 (refs. <sup>51,52</sup>), Akti-46 (ref. <sup>53</sup>), PP-hydroxyl<sup>54</sup>, sorafenib<sup>55</sup>, and JG-4 (ref. <sup>56</sup>) with minor adjustments made for synthetic tractability. After initial pilot syntheses and validation, compounds were synthesized by Pharmaron, Inc. Louisville KY. Couplings were performed overnight at room temperature (20–25 °C) on a rotator. Beads and compounds were mixed in 1:1 of dimethyl formamide:ethanol with 0.1 M 1-ethyl-3-(3-dimethylaminopropyl)carbodiimide.

After 24-h treatment with drug or DMSO, cell lysates were diluted in binding buffer with 1 mol/L NaCl, and kinase enrichment was performed using gravity chromatography following preclearing. After washing, the bound kinases were eluted with SDS followed by extraction/precipitation, tryptic digest and desalting. Liquid chromatography–tandem mass spectrometry (LC–MS/MS) was performed on a Velos Orbitrap (Thermo Scientific) with in-line high-performance liquid chromatography (HPLC) using an EASY-spray column (Thermo Scientific). Peptide identifications were made using ProteinProspector (v5.10.10) and input into Skyline for label-free quantification<sup>57</sup>.

Peptide quantification data were pre-processed before analysis with MSstats v2.3.3 (ref. <sup>58</sup>). First, library peptides and peptides that map to nonkinase proteins were removed. Kinase peptide peak area values were  $\log_2$ -transformed and quantile-normalized to correct for variation between replicates. Finally, peptides that mapped to multiple kinases were removed, as well as peptides that were entirely missing in one or more conditions. For each kinase, the  $\log_2$  ratio of each drug-treated condition to the DMSO control was estimated using the mixed-effects regression model in MSstats.

**Drug combination studies.** Cell lines were seeded in 384-well assay plates at a density of 1,000 cells/well in a total volume of 40  $\mu$ L/well and incubated at 37 °C, 5% CO<sub>2</sub> overnight. Dose matrices were assembled containing six-point, four-fold serial dilutions from the top concentration for each agent on the *x*- and *y*-axes. Following 72 h of drug exposure, proliferation and cell death was measured by staining with Hoescht (Life Technologies) nuclear dye and YO-PRO-1 (Life Technologies), respectively, and analyzed using a Thermo CellInsight High Content microscope. Raw phenotype measurements from each treated well were normalized to the median of vehicle-treated control wells and examined for synergistic effects between both compounds.

To evaluate drug combinations, we used a Loewe model of drug additivity and calculated a synergy score. First, we fit a sigmoidal function to each of the single-agent responses. Next, we calculated the expected inhibition for each combination using the Loewe additivity model<sup>20</sup>. The synergy score *S* was calculated as previously defined<sup>59</sup> as a positive-gated inhibition-weighted volume over of Loewe additivity:

$$S = \ln f_X \ln f_Y \sum \max(0, I_{\text{data}}) \max(0, I_{\text{data}} - I_{\text{Loewe}})$$

Where  $f_X$  and  $f_Y$  are the dilution factors used for compounds *X* and *Y*, respectively,  $I_{\text{data}}$  is the matrix of inhibition data at this dilution factor, and  $I_{\text{Loewe}}$  is the expected inhibition according to Loewe additivity. Synergy score calculations were also derived using Bliss independence<sup>20</sup>, based on a model in which drugs act independently of each other.  $CI_{50}$  values for equal-dose combinations were calculated as previously defined<sup>20</sup>:

$$CI_{50} = \frac{(D)_1}{(D_{50})_1} + \frac{(D)_2}{(D_{50})_2}$$

Where  $(D)_1$  and  $(D)_2$  are the given doses of the two drugs, and  $(D_{50})_1$  and  $(D_{50})_2$  are the  $IC_{50}$  values for each drug as a single agent.

To determine a cutoff for the synergy score, we simulated the distribution of scores generated by an additive drug combination. We generated two hypothetical

compounds by sampling random shape parameters for their dose–response functions and calculated the expected Loewe model of the combination. We then added normally distributed noise to the model with variance estimated from our experimental data and calculated the resulting synergy score. This process was repeated 100,000 times to simulate the distribution of synergy scores for different additive combinations. The 95<sup>th</sup> percentile of this distribution was 0.91 and so we conservatively identified combinations with  $S \geq 1$  as synergistic.

**Western blotting and antibodies.** Proteins were extracted using RIPA buffer (50 mM Tris–HCl pH 7.5, 150 mM NaCl, 0.1% sodium deoxycholate, 0.1% SDS, 1 mM EDTA pH 8.0, 1% NP-40) containing proteinase (Roche) and phosphatase (Roche) inhibitor cocktails. Samples were resolved using 4–12% SDS–PAGE gels (Life Technologies) and transferred to PVDF membranes (Millipore). Membranes were probed overnight on a 4 °C shaker with primary antibodies (1:1,000 dilution unless indicated) recognizing the following proteins: p-AKT (Ser473) (9271, Cell Signaling), AKT (4691, Cell Signaling), p-S6 (Ser240/244) (5364, Cell Signaling, 1:20,000), p-4E-BP1 (Thr37/46) (2855, Cell Signaling), p-AURKA (Thr288) (3079, Cell Signaling), AURKA (4718, Cell Signaling), Cleaved PARP (Asp214) (9541, Cell Signaling), BCL2 (2870, Cell Signaling), BAX (2772, Cell Signaling), MYC (ab32072, Abcam), and  $\beta$ -actin (3700, Cell Signaling).

**Mouse xenograft studies.** All animal studies were conducted in compliance with all relevant ethical regulations set forth by the UCSF Institutional Animal Care and Use Committee (IACUC). 4-week old immunocompromised NOD/SCID female mice were purchased from Taconic Biosciences, and MCF7 cells used for in vivo transplant were obtained from the UCSF Preclinical Therapeutics Core. Xenograft tumors were initiated in the cleared mammary fat pads of mice bearing slow release estrogen pellets (Innovative Research of America) by orthotopic injection of  $1 \times 10^6$  MCF7 cells in a 1:1 mixture of serum-free medium and Matrigel (BD Biosciences). When tumors reached  $\geq 1$  cm in any direction via electronic caliper measurements, mice were randomized into cohort groups and treatment was initiated.

Treatment arms received either vehicle (1:1 mixture of single-agent diluents), RAD001 formulated as a microemulsion (2 mg/kg/q; 30% propylene glycol, 5% Tween 80), MLN8237 (10 mg/kg/q; 10% 2-hydroxypropyl- $\beta$ -cyclodextrin, 1% sodium bicarbonate), or the combination daily via oral gavage. Animals were monitored daily for evidence of toxicity, including weight and skin effects, and changes in tumor size (mm<sup>3</sup>) through bidirectional measurements of perpendicular diameters using electronic calipers, and calculated as  $V = 1/2(\text{length} \times \text{width}^2)$ . Mice were sacrificed after 15 d of treatment, following which tumors were excised and a portion of the tissue fixed in 4% paraformaldehyde. The remaining tumor tissue was flash-frozen in liquid nitrogen.

**Immunohistochemical analysis.** PFA-fixed tumor samples were paraffin-embedded, and immunohistochemical staining of tissue sections was performed. TUNEL staining was carried out using the ApopTag Peroxidase In situ Apoptosis Detection Kit (Millipore) according to the manufacturer's instructions ( $n = 15$  data points per group; five high-powered (20 $\times$ ) fields analyzed from separate areas of each tumor from 3 mice per experimental group). Stained slides were digitized using the Leica DMi1 Microscope (Leica Microsystems) with a 20 $\times$  objective. Images were scored as the number of TUNEL-positive cells per captured field, and quantification was performed in a manner that was blinded to treatment group.

**Real-time PCR.** RNA was isolated according to the manufacturer's instructions (TRIzol, Life Technologies). One microgram of total RNA from each sample was subjected to first-strand cDNA synthesis according to the manufacturer's recommendations (Promega). Quantitative PCR was performed on a CFX96 Real-Time PCR detection system with a PrimeTime Gene Expression Master Mix (IDT technology) according to the manufacturer's protocol. AURKA was amplified with the following primers: 5'-AGTGGCAAACGCTCTGTCT-3' (forward primer) and 5'-GTGCCACACATTGTGGTTCT-3' (reverse primer). RPL13A was used as an endogenous control with the following primers: 5'-CGGATTTGGTCGTATTGG-3' (forward primer) and 5'-TCCTGGAAGATGGTGATG-3' (reverse primer). The cycling conditions for AURKA and RPL13A were as follows: one cycle at 95 °C for 3 min; 40 cycles of 95 °C for 15 s, and 60 °C for 60 s. The specificity of the PCR amplification was validated by the presence of a single peak in the melting curve analyses.

**Gene Set Enrichment Analyses (GSEA).** Gene set enrichment analysis (GSEA) of hallmark cancer gene signatures in the Molecular Signatures Database (MSigDB v6.0) was performed using GSEA v3.0 software (<http://www.broadinstitute.org/gsea/>)<sup>19</sup> under the following parameters: permutation, phenotype; metric, Signal2Noise; scoring scheme, weighted; and number of permutations, 1,000. Gene sets were considered significantly enriched following a nominal  $P < 0.05$  and FDR  $< 0.25$  cutoff.

**Statistical analysis.** Data are expressed as means  $\pm$  s.d., unless otherwise indicated. Statistical analyses were performed using GraphPad Prism 6 (v6.0.g) and R (v3.32). Two-tailed Student *t*-tests (with unequal variance) were used in all comparisons

unless otherwise noted.  $P < 0.05$  was considered statistically significant throughout the study.

**Reporting Summary.** Further information on experimental design is available in the Nature Research Reporting Summary linked to this article.

**Data availability.** All data generated or analyzed during this study are included in this published article and its supplementary information files. The raw mass spectrometry data is accessible via <http://prospector2.ucsf.edu/prospector/cgi-bin/msform.cgi?form=msviewer> under the search key: *lixlgarvea*.

## References

50. Neve, R. M. et al. A collection of breast cancer cell lines for the study of functionally distinct cancer subtypes. *Cancer Cell* **10**, 515–527 (2006).
51. Barvian, M. et al. Pyrido[2,3-d]pyrimidin-7-one inhibitors of cyclin-dependent kinases. *J. Med. Chem.* **43**, 4606–4616 (2000).
52. Daub, H. et al. Kinase-selective enrichment enables quantitative phosphoproteomics of the kinome across the cell cycle. *Mol. Cell* **31**, 438–448 (2008).
53. Blake, J. F. et al. Discovery of pyrrolopyrimidine inhibitors of Akt. *Bioorg. Med. Chem. Lett.* **20**, 5607–5612 (2010).
54. Tanaka, M. et al. An unbiased cell morphology-based screen for new, biologically active small molecules. *PLoS Biol.* **3**, e128 (2005).
55. Bankston, D. et al. A scaleable synthesis of BAY 43–9006: a potent Raf kinase inhibitor for the treatment of cancer. *Org. Process Res. Dev.* **6**, 777–781 (2002).
56. Statsuk, A. V. et al. Tuning a three-component reaction for trapping kinase substrate complexes. *J. Am. Chem. Soc.* **130**, 17568–17574 (2008).
57. MacLean, B. et al. Skyline: an open source document editor for creating and analyzing targeted proteomics experiments. *Bioinformatics* **26**, 966–968 (2010).
58. Choi, M. et al. MSstats: an R package for statistical analysis of quantitative mass spectrometry-based proteomic experiments. *Bioinformatics* **30**, 2524–2526 (2014).
59. Lehar, J. et al. Synergistic drug combinations tend to improve therapeutically relevant selectivity. *Nat. Biotechnol.* **27**, 659–666 (2009).

## Life Sciences Reporting Summary

Nature Research wishes to improve the reproducibility of the work that we publish. This form is intended for publication with all accepted life science papers and provides structure for consistency and transparency in reporting. Every life science submission will use this form; some list items might not apply to an individual manuscript, but all fields must be completed for clarity.

For further information on the points included in this form, see [Reporting Life Sciences Research](#). For further information on Nature Research policies, including our [data availability policy](#), see [Authors & Referees](#) and the [Editorial Policy Checklist](#).

### ▶ Experimental design

#### 1. Sample size

Describe how sample size was determined.

For in vivo experiments each arm contained at least 6 mice which we estimated to provide 90% power to detect a 20% difference in growth rate at P value < 0.05.

#### 2. Data exclusions

Describe any data exclusions.

For Fig. 1d one outlier data point was removed and is stated in the figure legend as the following text:

"Comparison of kinase activity ratios in BT549 and MCF7 cells treated with 100nM PD0325901 versus DMSO. Data represent 75 kinases with one outlier kinase (GAK, BT549 log2 fold change 8.3) removed."

#### 3. Replication

Describe whether the experimental findings were reliably reproduced.

Experimental findings were successfully reproduced. Western blots were reproduced a minimum of 3 times with the exception of Fig. 5a detailing analysis of xenograft tumor specimens.

#### 4. Randomization

Describe how samples/organisms/participants were allocated into experimental groups.

For mouse xenograft studies, mice were randomized into control and treatment cohort groups when tumors reached  $\geq 1$ cm in any direction via electronic caliper measurements.

#### 5. Blinding

Describe whether the investigators were blinded to group allocation during data collection and/or analysis.

Quantification of TUNEL staining from mouse xenograft studies was performed in a manner that was blinded to treatment group. For remaining studies in the manuscript, the authors were not blinded to data collection and analysis.

Note: all studies involving animals and/or human research participants must disclose whether blinding and randomization were used.

## 6. Statistical parameters

For all figures and tables that use statistical methods, confirm that the following items are present in relevant figure legends (or in the Methods section if additional space is needed).

n/a Confirmed

- The exact sample size ( $n$ ) for each experimental group/condition, given as a discrete number and unit of measurement (animals, litters, cultures, etc.)
- A description of how samples were collected, noting whether measurements were taken from distinct samples or whether the same sample was measured repeatedly
- A statement indicating how many times each experiment was replicated
- The statistical test(s) used and whether they are one- or two-sided (note: only common tests should be described solely by name; more complex techniques should be described in the Methods section)
- A description of any assumptions or corrections, such as an adjustment for multiple comparisons
- The test results (e.g.  $P$  values) given as exact values whenever possible and with confidence intervals noted
- A clear description of statistics including central tendency (e.g. median, mean) and variation (e.g. standard deviation, interquartile range)
- Clearly defined error bars

See the web collection on [statistics for biologists](#) for further resources and guidance.

## ► Software

Policy information about [availability of computer code](#)

### 7. Software

Describe the software used to analyze the data in this study.

Statistical analyses for this study were performed using GraphPad Prism 6 (v6.0g) and R (v3.32). Gene set enrichment analysis was performed using GSEA software (v3.0) available at <http://www.broadinstitute.org/gsea/>.

For manuscripts utilizing custom algorithms or software that are central to the paper but not yet described in the published literature, software must be made available to editors and reviewers upon request. We strongly encourage code deposition in a community repository (e.g. GitHub). *Nature Methods* [guidance for providing algorithms and software for publication](#) provides further information on this topic.

## ► Materials and reagents

Policy information about [availability of materials](#)

### 8. Materials availability

Indicate whether there are restrictions on availability of unique materials or if these materials are only available for distribution by a for-profit company.

All materials are available from standard commercial sources.

### 9. Antibodies

Describe the antibodies used and how they were validated for use in the system under study (i.e. assay and species).

Primary antibodies used in this study are reported as (catalog number, supplier) and recognize the following proteins:

p-AKT (Ser473) (9271, Cell Signaling), AKT (4691, Cell Signaling), p-S6 (Ser240/244) (5364, Cell Signaling), p-4E-BP1 (Thr37/46) (2855, Cell Signaling), p-AURKA (Thr288) (3079, Cell Signaling), AURKA (4718, Cell Signaling), Cleaved PARP (Asp214) (9541, Cell Signaling), BCL2 (2870, Cell Signaling), BAX (2772, Cell Signaling), c-MYC (ab32072, Abcam), and  $\beta$ -actin (3700, Cell Signaling).

All antibodies were validated for the indicated use by the manufacturer available on their website. See Methods.

## 10. Eukaryotic cell lines

a. State the source of each eukaryotic cell line used.

BT549, and SKBR3 cells were obtained from the UCSF Cell Culture Facility. BT474, BT20, HCC1428, HCC38, LY2, MCF7, MDAMB231, MDAMB453, T47D, SUM52PE, and ZR75B cell lines were obtained from the American Type Culture Collection (ATCC).

b. Describe the method of cell line authentication used.

Cell lines used for proteomic profiling and molecular analyses were authenticated by STR analysis.

c. Report whether the cell lines were tested for mycoplasma contamination.

All cell lines tested negative for mycoplasma contamination.

d. If any of the cell lines used are listed in the database of commonly misidentified cell lines maintained by [ICLAC](#), provide a scientific rationale for their use.

No commonly misidentified cell lines were used in this study.

## ► Animals and human research participants

Policy information about [studies involving animals](#); when reporting animal research, follow the [ARRIVE guidelines](#)

## 11. Description of research animals

Provide details on animals and/or animal-derived materials used in the study.

For mouse xenograft studies, 4-week old immunocompromised NOD/SCID female mice were purchased from Taconic Biosciences.

Policy information about [studies involving human research participants](#)

## 12. Description of human research participants

Describe the covariate-relevant population characteristics of the human research participants.

The study did not involve human research participants.